THE JOURNAL OF BIOLOGICAL CHEMISTRY VOL. 286, NO. 15, pp. 13470–13480, April 15, 2011

Distinct Molecular Regulation of Glycogen Synthase Kinase-3α Isozyme Controlled by Its N-terminal Region

FUNCTIONAL ROLE IN CALCIUM/CALPAIN SIGNALING[*S]

Received for publication, March 30, 2010, and in revised form, January 20, 2011 Published, JBC Papers in Press, January 25, 2011, DOI 10.1074/jbc.M110.127969

Inbar Azoulay-Alfaguter[‡1,2], Yakey Yaffe[§1], Avital Licht-Murava[‡], Malgorzata Urbanska[¶], Jacek Jaworski[¶], Shmuel Pietrokovski[‖3], Koret Hirschberg[§], and Hagit Eldar-Finkelman[‡4]

From the Departments of [‡]Human Molecular Genetics and Biochemistry and [§]Pathology, Sackler School of Medicine, Tel Aviv University, Tel Aviv 69978, Israel, the [¶] International Institute of Molecular and Cell Biology, Warsaw 02-109, Poland, and the [‖]Department of Molecular Genetics, the Weizmann Institute of Science, Rehovot 76100, Israel

Glycogen synthase kinase-3 (GSK-3) is expressed as two isozymes α and β. They share high similarity in their catalytic domains but differ in their N- and C-terminal regions, with GSK-3α having an extended glycine-rich N terminus. Here, we undertook live cell imaging combined with molecular and bioinformatic studies to understand the distinct functions of the GSK-3 isozymes focusing on GSK-3α N-terminal region. We found that unlike GSK-3β, which shuttles between the nucleus and cytoplasm, GSK-3α was excluded from the nucleus. Deletion of the N-terminal region of GSK-3α resulted in nuclear localization, and treatment with leptomycin B resulted in GSK-3α accumulation in the nucleus. GSK-3α rapidly accumulated in the nucleus in response to calcium or serum deprivation, and accumulation was strongly inhibited by the calpain inhibitor calpeptin. This nuclear accumulation was not mediated by cleavage of the N-terminal region or phosphorylation of GSK-3α. Rather, we show that calcium-induced GSK-3α nuclear accumulation was governed by GSK-3α binding with as yet unknown calpain-sensitive protein or proteins; this binding was mediated by the N-terminal region. Bioinformatic and experimental analyses indicated that nuclear exclusion of GSK-3α was likely an exclusive characteristic of mammalian GSK-3α. Finally, we show that nuclear localization of GSK-3α reduced the nuclear pool of β-catenin and its target cyclin D1. Taken together, these data suggest that the N-terminal region of GSK-3α is responsible for its nuclear exclusion and that binding with a calcium/calpain-sensitive product enables GSK-3α nuclear retention. We further uncovered a novel link between calcium and nuclear GSK-3α-mediated inhibition of the canonical Wnt/β-catenin pathway.

Glycogen synthase kinase-3 (GSK-3)[5] is a highly conserved serine/threonine kinase that is ubiquitously distributed in eukaryotes. GSK-3 is a constitutively active enzyme that modulates diverse cellular functions, including metabolism, development, cell survival, and mood behavior (1–3). Activated GSK-3 phosphorylates numerous substrates in various cell compartments, and deregulation of its activity has been implicated in the pathogenesis of human diseases such as type 2 diabetes and certain neurodegenerative and psychiatric disorders (4–10). GSK-3 has thus become an important target for drug discovery and its cellular regulation is of major interest.

Mammalian GSK-3 exists in two distinct isoforms, α and β, each encoded by separate genes that share 98% sequence identity in their catalytic domains and 84% identity overall (11). The specific roles of the two GSK-3 isoforms are not yet fully understood, although it appears that they are not functionally identical as initially described (12). The GSK-3 isoforms share both common and distinct biological activities. For example, whereas GSK-3α-knock-out mice are viable and fertile, disruption of GSK-3β is lethal at an early embryonic stage (13, 14). Mice lacking GSK-3α display improved glucose tolerance and increased glycogen synthesis compared with tissue-specific GSK-3β knock-outs (14, 15). GSK-3α has been shown to regulate amyloidogenic processing of Alzheimer amyloid precursor protein (16). GSK-3α and β also have distinct functions in cardiac cell differentiation and proliferation (17, 18) and have opposite effects on certain transcription factors (19). In some cases, however, the isoforms show redundant activity; for example, the isoforms have similar effects on phosphorylation and destabilization of β-catenin (20) and regulation of axonal growth (21, 22). In a different study GSK-3 isoforms were shown to be subjected to N-terminal cleavage by the calcium-dependent cysteine protease calpain (23). Calpains are a large family of calcium-dependent intracellular proteases that play integral regulatory roles in various signaling pathways (for review, see Ref. 24). Aberrant activation of calpains is observed in a variety of pathological conditions (25–27). Calcium/calpain signaling was shown to regulate β-catenin (28–30), a multifunctional protein serving both as a structural component and a signaling component of the Wnt signaling pathway (31, 32). Phosphorylation of β-catenin by GSK-3 enhances its proteosomal degradation and reduces its transcriptional activity (33–35). The signaling networks linking calpains and GSK-3 with the canonical Wnt/β-catenin pathway have not been elucidated.

* This work was supported by Seventh Framework Program (FP7) European Union Grant 223276 "NeuroGSK3" and Israeli Academy of Sciences Grant 341/10.

[S] The on-line version of this article (available at http://www.jbc.org) contains Table S1, Figs. S1–S3, and Movie S1.

[1] Both authors contributed equally to this work.

[2] This work was submitted in partial fulfillment of the requirements for a Ph.D. at Sackler School of Medicine, Tel Aviv University.

[3] Holds a Hermann and Lilly Schilling Foundation chair.

[4] To whom correspondence should be addressed. Fax: 972-3-640-8749; E-mail: heldar@post.tau.ac.il.

[5] The abbreviation used is: GSK-3, glycogen synthase kinase-3.

The molecular basis for the distinct functions of GSK-3 isoforms is largely unknown. Despite significant homology, GSK-3 isoforms do differ significantly in their N and C termini. GSK-3α, which is the larger protein, has an extended glycine-rich N-terminal region (11) that is thought to function as a pseudosubstrate (36). We hypothesized that the N-terminal domain of GSK-3α might contribute to localization, targeting, and protein-protein interactions unique to this isoform. Here, we undertook live cell imaging combined with molecular and bioinformatics studies to uncover the role of the N terminus of GSK-3α.

EXPERIMENTAL PROCEDURES

Materials—Anti-GSK-3α and anti-cyclin D1 antibodies were from Santa Cruz Biotechnology (Santa Cruz, CA); anti-phosphoserine 21-GSK-3α and anti-GFP antibodies were from Cell Signaling Technologies (Beverly, MA). Anti-GSK-3β and anti-β-catenin antibodies were from Transduction Laboratories (Franklin Lakes, NJ). ABC antibody was from Millipore (Billerica, MA). Ionomycin, calpeptin, and MG132 were from Calbiochem. The cDNA encoding GSK-3α in an pMT2 vector was kindly provided by Dr. J. Woodgett (Samuel Lunenfeld Research Institute, Toronto, ON, Canada), and the cDNA GFP-tagged γ-tubulin was a gift from Dr. Q. Gao (Northwestern University, Evanston, IL). All other reagents were from Sigma.

Plasmids—GSK-3α cDNA was generated by PCR from plasmid pMT2-GSK-3α and subcloned into the vector pEGFP-N1 (Invitrogen) at EcoRI and BamHI sites. GSK-3β was subcloned into pEGFP-N1 at the KpnI and SmaI sites. ΔN-GSK-3α-GFP (the kinase lacking the first 63 amino acids) was generated by PCR from the pMT2 plasmid, and the GSK-3α cDNA fragment was digested with EcoRI and BamHI and subcloned into pEGFP-N1. N′-GSK-3α-GFP (coding for amino acids 1–63 of GSK-3α) was generated by PCR. The PCR fragment was digested with EcoRI and XhoI and subcloned into vector pEGFP-N2 (Invitrogen). GSK-3α-mCherry was generated by digesting GSK-3α from GSK-3α-pEGFP-N1 with EcoRI and BamHI and subcloning into plasmid mCherry-N1 (Invitrogen). *Danio rerio* GSK-3α was generated by PCR using GSK-3α-pCMV SPORT 6.1 (Open Biosystems, Huntsville, AL) as the template. The PCR product was digested with XhoI and EcoRI and subcloned into pEGFP-N2. All new constructs were sequenced. Sequences of primers used are available from the authors upon request.

Cell Culture and Transfections—COS-7 cells (African green monkey) (37) were maintained in Dulbecco's modified Eagle's medium (DMEM) supplemented with 10% fetal calf serum (FCS), 5 mg/ml glutamine, and 1% streptomycin in a 37 °C humidified 5% CO_2 incubator. The cells were transiently transfected with the indicated constructs (2–7 μg) using FuGENE6 (Roche Applied Science) according to the manufacturer's protocol. Cells were imaged 24 h after transfection. Cells were harvested for Western blot analysis 24 or 48 h after transfection.

Cell Extraction and Subcellular Fractionation—Cells were collected and lysed in ice-cold buffer G (20 mM Tris, pH 7.5, 10 mM β-glycerophosphate, 10% glycerol, 1 mM EGTA, 1 mM EDTA, 50 mM NaF, 5 mM sodium pyrophosphate, 0.5 mM orthovanadate, 1 mM benzamidine, 5 μg/ml leupeptin, 25 μg/ml aprotinin, 5 μg/ml pepstatin, and 0.5% Triton X-100). Cell extracts were centrifuged at 1,000 × *g* for 10 min to obtain the cytosolic fraction. The pellet containing the nuclei was washed three times with ice-cold buffer H (150 mM β-glycerophosphate, pH 7.3, 50% glycerol, 5 mM EGTA, 5 mM EDTA, 40 mM NaF, 25 mM sodium pyrophosphate, 25 μg/ml leupeptin, 25 μg/ml aprotinin, 1 mM DTT, and 0.1% Triton X-100) and sonicated using an X2 Ultrasonic processor (Misonix, Farmingdale, NY). Protein concentration of the cytosolic fraction was determined by Bradford assay. Equal amounts of protein (30–50 μg) were subjected to gel electrophoresis (10% polyacrylamide), transferred to nitrocellulose membranes, and immunoblotted with the indicated antibodies.

Live Cell Microscopy Analysis—Fluorescent images were obtained by confocal laser scanning microscopy (LSM model PASCAL or 510 META with an Axiovert 200 microscope; Carl Zeiss MicroImaging). Fluorescence emissions resulting from excitations of 488 nm for GFP and 543 nm for mCherry or DiHcRED were detected using filter sets supplied by the manufacturer. Throughout the procedure, cells were imaged in DMEM lacking phenol red, in buffer including 20 mM HEPES, pH 7.4, and kept at 37 °C on the microscope stage using an electronic temperature-controlled airstream incubator. Transfection and imaging were carried out in Labtek chambers (Nunc, Naperville, IL). The confocal and time-lapse images were captured using a Plan-Apochromat 63 NA 1.4 objective (Carl Zeiss MicroImaging). Images and movies were generated and analyzed using the Zeiss LSM software and National Institutes of Health Image and ImageJ software. In addition, the autofocusing function integrated into the "advanced time series" macro set (Carl Zeiss MicroImaging) was used. Photobleaching of GSK-3β-GFP was performed using 5–20 scans with the 488- or 543-nm laser lines at full power in a rectangular region in the nucleus. Pre- and post-bleach images were captured using low laser intensity. Fluorescence recovery in the bleached region during the time series was quantified using LSM software (Carl Zeiss MicroImaging). For figure preparation, images were processed with Photoshop (Adobe, San Jose, CA) using brightness, contrast, and gamma corrections to accommodate the 12- to 8-bit transition of the digital files.

Bioinformatics Analysis—Sequence searches were performed in the NCBI databases using the BLAST programs (38), and identified GSK-3 sequences were aligned to each other using BLASTp, MEME (39), and GLAM-2 (40) programs. Sequence logos were created as described previously (41).

Primary Neuron Cultures and Immunofluorescence Staining—Primary hippocampal cultures were prepared from embryonic day 18 rat brains as described previously (42). Cells were plated on coverslips coated with poly-L-lysine (30 μg/ml; Sigma) and laminin (2 μg/ml; Roche Applied Science) at densities of 500 and 1,250 cells/mm^2 for hippocampal and cortical neurons, respectively. Neuronal cultures were grown in Neurobasal medium (Invitrogen) supplemented with B27 (Invitrogen), 0.5 mM glutamine, 12.5 μM glutamate, and penicillin/streptomycin mix (Sigma). On day 21 of *in vitro* culture, neurons were treated with 5 μM ionomycin (Calbiochem), 2 μM thapsigargin (Sigma), or KCl to induce an increase in intracellular calcium ion levels. Ionomycin and thapsigargin were applied to cells in buffer con-

taining 20 mM HEPES, pH 7.4, 150 mM NaCl, 1 mM $MgCl_2$, 2.7 mM KCl, 25 mM glucose, 1 mM Na_2HPO_4, 2% bovine serum albumin (BSA) for 30 and 45 min, respectively. For KCl stimulation, neurons were first incubated for 5 min in low KCl buffer (5 mM KCl, 20 mM HEPES, pH 7.4, 150 mM NaCl, 15 mM $MgCl_2$, 1.5 mM $CaCl_2$, 30 mM glucose), then transferred to high KCl concentration (same conditions except for 90 mM KCl) for 1 min, and finally returned to low KCl for 30 s. This treatment was followed by two additional cycles of high and low KCl exposure. Cells were then washed with Neurobasal medium and incubated in conditioned medium for 30 min.

For immunofluorescent staining, neurons were fixed with 4% paraformaldehyde containing 4% sucrose in PBS for 10 min at room temperature. After fixation, cells were washed three times with PBS for 5 min at room temperature and incubated with primary mouse anti-GSK-3α antibody in GDB buffer (0.2% gelatin, 0.8 M NaCl, 0.5% Triton X-100, 30 mM phosphate buffer, pH 7.4) overnight at 4 °C. Cells were then washed three times in PBS for 10 min at room temperature. Secondary Alexa Fluor 488-conjugated antibody (Invitrogen) was applied in GDB buffer for 1 h at room temperature. Cells were then washed three times with PBS for 10 min each. Nuclei were counterstained with Hoechst 33258 stain (bisbenzimide; Sigma). Confocal images of cells were obtained with sequential acquisition settings at the maximal 1,024 × 1,024 pixel resolution of the Zeiss LSM 5 Exciter microscope. Each image was a *z*-series of images, each averaged two times.

Statistical Analysis—Data were analyzed with Origin Professional 6.0 software using Student's *t* test to analyze densitometry data. Data were considered significant at $p < 0.05$.

RESULTS

GSK-3α/β Isoforms Show Distinct Cellular Distributions—Because the catalytic domains of GSK-3α and GSK-3β are very similar, we hypothesized that their different functions might be associated with distinct subcellular localization (under either basal or stimulated conditions). GSK-3α and β constructs tagged with GFP at their C termini (termed GSK-3α/β-GFP) were used to determine cellular localization. COS-7 cells were transiently co-transfected with GSK-3α-GFP and GSK-3β-GFP plasmids together with the pmCherry-N1 vector, which served as a control. Live cells were imaged by confocal microscopy. GSK-3α-GFP was found in the cytoplasm and was excluded from the cell nucleus, as shown in representative images (Fig. 1*A*, *upper panel*). In contrast, GSK-3β-GFP (Fig. 1*A*, *lower panel*) was observed in both the cytoplasm and the nucleus. Cells expressing the GSK-3-GFP isoforms were subjected to cytoplasmic/nuclear subcellular fractionation, and fractions were immunoblotted and probed with GFP antibody. Consistent with the cell imaging results, GSK-3β-GFP was detected in both the nuclear and cytoplasmic fractions, whereas GSK-3α-GFP was found primarily in the cytoplasmic fraction (Fig. 1*B*). Using anti-GSK-3α antibody or DiHcRED-tagged histone (37) for nuclear localization in a cell imaging study gave comparable results (Figs. 2*A* and 4*A* and supplemental Fig. S1*A*). Analysis of expression patterns of endogenous GSK-3 proteins in COS-7, epithelial HT29, and SH-SH5Y neuroblastoma cell lines gave corroborating results (Fig. 1*C*). Fluorescence recovery after photobleaching was applied to study the transport of GSK-3β-GFP between the cytosol and the nucleus. A region of interest within the nuclei of cells expressing GSK-3β-GFP was photobleached, and the recovery of fluorescence representing the exchange between cytosol and nucleus confirmed that GSK-3β shuttles between the two (Fig. S1*B*).

We next determined whether GSK-3 isoforms were differentially associated with cytoplasmic compartments or organelle membranes. COS-7 cells were co-transfected with GSK-3α-GFP or GSK-3β-GFP plasmids together with mCherry-tagged constructs expressing protein "markers" for the endoplasmic reticulum (VSVG-Δtm), Golgi (GalT), and plasma membranes (PM, VSVG) (37). In addition, GSK-3α tagged with mCherry protein (GSK-3α-mCherry) was co-expressed with GFP-tagged γ-tubulin (a centriole marker). The distribution of GSK-3α-GFP in the cytoplasm did not exhibit patterns or shapes identical to those observed for endoplasmic reticulum, Golgi, or cell surface membrane markers (Fig. 1*D*). On the other hand, GSK-3α-mCherry signal overlapped with the γ-tubulin-GFP marker for perinuclear centrioles (Fig. 1*D*, *bottom panel*). This localization was verified by *z*-section analysis (supplemental Fig. S1*C*). A similar distribution pattern was observed for the cytosolic fraction of GSK-3β-GFP.[6]

Deletion of the N Terminus of GSK-3α Results in Nuclear Localization—We next examined whether cytoplasmic retention of GSK-3α is controlled by its extended glycine-rich N-terminal domain. Two GSK-3α mutants were generated (Fig. 2*A*). Approximately half of the N-terminal domain, the first 63 amino acids, was deleted from the GFP-tagged or nontagged GSK-3α constructs yielding a protein comparable in length to that of GSK-3β; these constructs are termed ΔN-GSK-3α. The second mutant encoded the first 63 amino acids of the N-terminal domain (termed here N′-GSK-3α-GFP). Both constructs were expressed in COS-7 cells together with DiHcRED-histone, and living cells were imaged by confocal microscopy. Unlike the "full-length" GSK-3α-GFP, ΔN-GSK-3α-GFP was localized in the nucleus (Fig. 2*B*), whereas the N′-GSK-3α-GFP fragment was distributed diffusely throughout the cells (Fig. 2*B*). Subcellular fractionation of cells expressing ΔN-GSK-3α-GFP, ΔN-GSK-3α, and N′-GSK-3α-GFP gave results consistent with the microscopy data (Fig. 2*C*). Hence, the N-terminal region controls GSK-3α nuclear localization.

We next examined whether the N-terminal region prevents GSK-3α entry into the nucleus. The cells were treated with leptomycin B, a specific inhibitor of the CRM1/exporting nuclear export system. This resulted in nuclear accumulation of GSK-3α-GFP (Fig. 2*D*), indicating that GSK-3α-GFP has the ability to enter the nucleus. Taken together, we concluded that once in the nucleus GSK-3α is rapidly transported out. This transport appears to be facilitated by the N-terminal region.

GSK-3α N-terminal Region Is Highly Conserved in Mammals—Bioinformatic analyses of the N-terminal regions of all known GSK-3α family proteins (supplemental Table S1) showed significant variability; in mammals, however, this region was highly conserved (Fig. 3*A*). This raised the possibility that the

[6] I. Azoulay-Alfaguter, unpublished data.

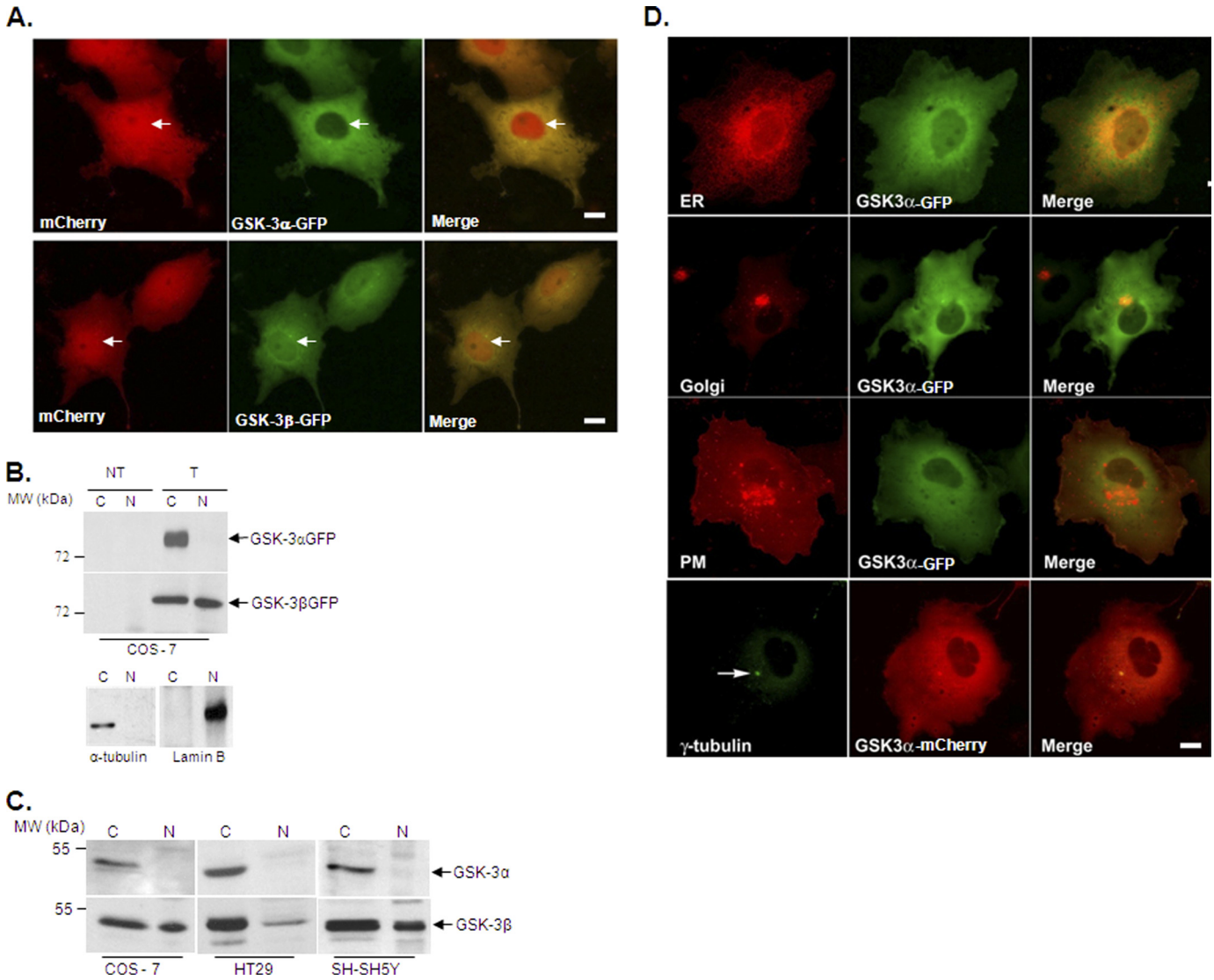

FIGURE 1. **Intracellular distribution of GSK-3α and GSK-3β.** *A*, COS-7 cells were transiently co-transfected with GSK-3α-GFP or GSK-3β-GFP constructs together with pmCherry-N1 vector, and live cells were imaged by confocal microscopy. Fluorescence of mCherry (*red*) and GFP (*green*), and the merged images are shown. *Scale bars*, 5 μm. *B*, COS-7 cells were transfected with GSK-3α-GFP or GSK-3β-GFP, and cells were then fractionated into nuclear (*N*) and cytosolic (*C*) fractions as described under "Experimental Procedures." Proteins were separated by gel electrophoresis and immunoblotted with anti-GFP or anti-GSK-3β antibody (*upper panel*). Nuclear and cytosolic fractions were verified, respectively, by lamin B (nuclear marker) and α-tubulin (cytosolic marker) localization as indicated in the *lower panel*. *NT*, nontransfected; *T*, transfected. *C*, endogenous GSK-3α was detected in cytoplasmic and nuclear fractions prepared from COS-7, HT29, and SH-SY5Y cells. *D*, COS-7 cells were transiently co-transfected with GSK-3α-GFP and mCherry-tagged constructs expressing protein markers for endoplasmic reticulum (*ER*; VSVG-ΔTM8), Golgi (GalT), and plasma membrane (*PM*; VSVG). Live cells were imaged by confocal microscopy. *Bottom panel* shows GSK-3αmCherry (*red*) co-expressed with the centriole marker γ-tubulin-GFP (*green*); *arrows* point to the centriole in the *bottom panel*. *Scale bars*, 10 μm.

observed cytoplasmic retention was specific to mammalian GSK-3α proteins. We therefore examined the cellular distribution of zebrafish GSK-3α. This protein has the extended N terminus of the GSK-3α isoforms typical of mammals, but has significant sequence differences (43) as shown in Fig. 3*B*. A zebrafish GSK-3α-GFP (ZGSK-3α-GFP) construct was generated and expressed in COS-7 cells. As shown in Fig. 3*C*, ZGSK-3α-GFP was detected in both the cytoplasm and the nucleus. Although not definitive, the experimental results with the zebrafish construct and the uniqueness of the N-terminal regions of all known mammalian GSK-3α proteins relative to GSK-3α N-terminal domains from other species suggest that mammalian GSK-3α isoforms are unique with respect to cellular localization.

Calpain Activation by Calcium Addition or Serum Deprivation Triggers Nuclear Accumulation of GSK-3α—Although our data indicated that GSK-3α was excluded from the cell nucleus, we hypothesized that it might accumulate in the nucleus after certain stimuli. Indeed, we found that treatment with calcium (1–5 mM) or a combination of calcium and the calcium ionophore ionomycin resulted in rapid nuclear accumulation of GSK-3α-GFP (Fig. 4*A* and supplemental Movie S1). This effect peaked between 30 and 60 min after calcium addition and was observed in most of the evaluated cells. The calpain inhibitor calpeptin strongly blocked this effect (Fig. 4*A*), suggesting that calpain-mediated protein proteolysis is essential for GSK-3α nuclear translocation. A similar rapid nuclear accumulation of GSK-3α-GFP was observed following serum deprivation (Fig.

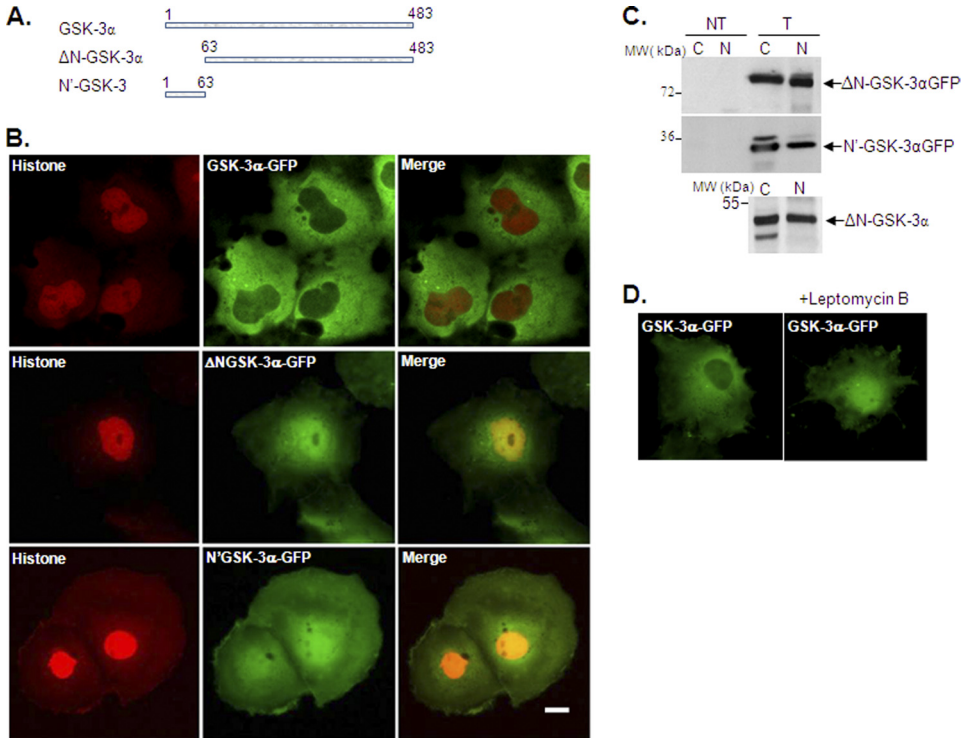

FIGURE 2. **Deletion of the N-terminal region of GSK-3α results in nuclear localization.** *A*, schematic presentation of GSK-3α constructs. *B*, COS-7 cells transiently co-transfected with GSK-3α-GFP, ΔN-GSK-3α-GFP, or N′-GSK-3α-GFP constructs together with DiHcRed-histone plasmid. Live cells were imaged by confocal microscopy. Fluorescence of DiHcRed, GFP, and the merged images is shown. *C*, cells transfected with ΔN-GSK-3α-GFP, nontagged ΔN-GSK-3α, and N′-GSK-3α-GFP. Cells were separated into nuclear (*N*) and cytosolic (*C*) fractions as described under "Experimental Procedures." Fractions were separated by gel electrophoresis and immunoblotted with anti-GFP or anti-GSK-3α antibody (for ΔN-GSK-3α, *lower panel*) as indicated. *NT*, nontransfected; *T*, transfected. *Scale bars*, 10 μm. *D*, COS-7 cells transfected with GSK-3α-GFP and treated with 20 nM leptomycin B for 2 h. Live cells were imaged by confocal microscopy. GFP fluorescence is shown.

4*B*), which might explain previous reports of nucleus-localized GSK-3α in serum-starved cells (44). Interestingly, serum starvation or calcium treatment did not abolish the localization of GSK-3α-GFP in the centrioles (supplemental Fig. S1*D*).

It has been suggested that calpain cleaves the N terminus from GSK-3 (23). We thus speculated that N-terminal truncation of GSK-3α is the likely mechanism for calcium-induced GSK-3α accumulation into the nucleus. However, we were unable to detect GSK-3α-GFP fragmentation in calcium-treated (Fig. 4*E*, *first 3 lanes*) or serum-starved cells (supplemental Fig. S2). This could be because the deletion from the N terminus was small and, therefore, not detectable by Western blot analysis. Alternatively, it is possible that GSK-3α fragments are unstable and rapidly degraded. To address these two possibilities, a GSK-3α construct was generated in which GFP was fused to the N terminus (GFP-GSK-3α). Consistent with our previous results, GFP-GSK-3α was observed in the cytoplasm under basal conditions but was localized to the nucleus when calcium was added to the medium (Fig. 4*C*). Cell fractionation and immunoblot analysis using an anti-GFP antibody confirmed that full-length GSK-3α-GFP (and not a truncated form as GFP signal remained) was translocated into the nucleus (Fig. 4*D*). No GSK-3α fragments were detected in immunoblot analyses using either anti-GSK-3α or anti-GFP antibody (Fig. 4, *D* and *E*, respectively); if this protein were cleaved, we would expect to see an ~55-kDa band. In addition, we examined whether endogenous or overexpressed GSK-3α were affected by calcium or serum starvation in SH-SY5Y neuroblastoma cells. In these experiments, truncation of GSK-3α was not detected (supplemental Fig. S2).

To address further the possibility that GSK-3α fragments are unstable, cells were treated with the proteasome inhibitor MG132 prior to the addition of calcium. No GSK-3α-GFP fragments were detected under these conditions (Fig. 4*F*). Furthermore, ΔN-GSK-3α-GFP was not degraded after calcium treatment, indicating that this fragment is stable (Fig. 4*G*). Thus, truncation of GSK-3α does not appear to be the mechanism responsible for its nuclear accumulation under these conditions. Finally, we demonstrated that Ca^{2+}-dependent (endogenous) GSK-3α accumulation in the nucleus was observed in primary hippocampal neurons. Upon treatment with various agents, including ionomycin, thapsigargin, and KCl, all known to induce increased intracellular levels of Ca^{2+}, GSK-3α was accumulated in the nucleus in this physiologically relevant system (Fig. 4*H*). A similar effect was observed in serum-starved neurons (supplemental Fig. S3).

N terminus Is Required for Calpain-mediated GSK-3α Accumulation in the Nucleus—We next examined possible mechanisms that may be responsible for GSK-3α nuclear localization. Because GSK-3α nuclear accumulation was not mediated by proteolysis (Fig. 4), we considered the possibility that GSK-3α binding with a calcium/calpain-dependent product governs it nuclear accumulation. If this hypothesis is correct, it should be possible to saturate these interactions by overexpressing either GSK-3α or the N-terminal region (if this region is required for such interactions). GSK-3α-GFP was co-expressed with GSK-

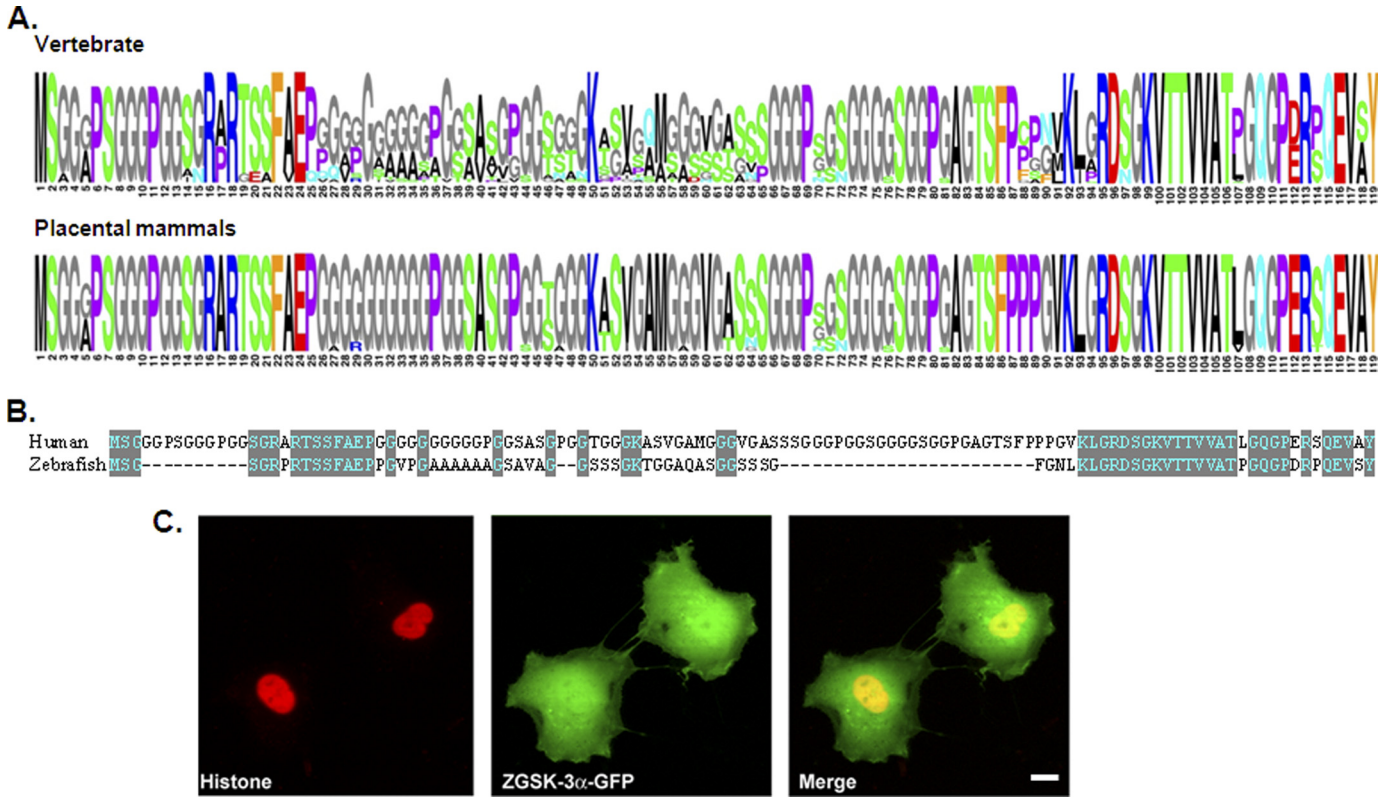

FIGURE 3. **N-terminal region of mammalian GSK-3α is highly conserved.** *A*, multiple sequence alignment of the N-terminal regions of the GSK-3α family (*top*) or mammalian GSK-3α (*bottom*) presented as sequence logos (41). *B*, sequence alignment of N-terminal regions of zebrafish GSK-3α and human GSK-3α. *C*, COS-7 cells transiently co-transfected with zebrafish GSK-3α-GFP and DiHcRED-histone plasmids. Live cells were imaged by confocal microscopy as described. Fluorescence of DiHcRED, GFP, and merged images are shown. *Scale bar*, 10 μm.

3α, and in addition, GSK-3α-mCherry was co-expressed with N′-GSK-3α-GFP. When cells were treated with calcium, the GFP or mCherry signal was not detected in the nucleus, indicating that nuclear accumulation of GSK-3α-GFP or GSK-3α-mCherry was blocked by overexpression of GSK-3α or its N-terminal domain, respectively (Fig. 5*A*). On the other hand, overexpression of ΔN-GSK-3α-GFP did not prevent calcium-induced GSK-3α-mCherry accumulation in the nucleus (Fig. 5*A*). These results supported our hypothesis that calcium-induced GSK-3α nuclear accumulation is mediated by GSK-3α binding with a (as yet unknown) calpain-sensitive product and that this binding is mediated by the N-terminal region. This generated complex likely "masks" the nuclear exclusion influence of the N-terminal region.

Phosphorylation of protein kinases is known to regulate their cellular distribution and their import/export from the nucleus (45–48). Phosphorylation of GSK-3α at serine 21, located within its N-terminal region, inhibits its kinase activity via its ability to function as a pseudosubstrate (49, 50). However, treatment of cells with okadaic acid, which enhanced serine 21 phosphorylation, did not promote GSK-3α-GFP or endogenous GSK-3α nuclear localization under basal conditions or after treatment with calcium (Fig. 5*B*). Hence, the "closed" conformational imposed by autophosphorylation (at Ser-21) does not contribute to GSK-3α nuclear localization. Similarly, phosphorylation at tyrosine 279, which enhances its catalytic activity (51), did not promote of GSK-3α-GFP or endogenous GSK-3α nuclear localization as judged by treating with sodium orthovanadate, a "general" tyrosine phosphatase (Fig. 5*C*).

The results with leptomycin B indicated that GSK-3α-GFP can enter the nucleus (Fig. 2*D*). Still, we wanted to verify that GSK-3α cytoplasmic retention was not governed by immobilization (*i.e.* binding to cytoplasmic anchors). If this were the mechanism, saturation with GSK-3α should compete with binding in the cytoplasm, and the "free" nonbound GSK-3α should be localized in the nucleus. COS-7 cells were transfected with increasing doses of GSK-3α-GFP plasmid. Overexpression of GSK-3α-GFP did not influence its cytoplasmic localization (Fig. 5*D*). Hence, we verified that GSK-3α-GFP cytoplasmic retention is not governed by cytoplasm anchors. Certainly, this does not refute the possibility that a certain fraction of GSK-3α/GSK-3α-GFP is bound to cytoplasmic proteins.

GSK-3α Down-regulates Nuclear β-Catenin Levels and Its Target Cyclin D1—Once in the nucleus, GSK-3α may activate multiple nuclear events, including phosphorylation, transcriptional activity, and protein export. β-Catenin is a key effector of the Wnt signaling pathway (31, 32) and a known substrate of GSK-3. Its phosphorylation by GSK-3 enhances its proteosomal degradation (33, 35, 52). We thus examined whether nuclear GSK-3α regulates nuclear β-catenin. We first expressed ΔN-GSK-3α-GFP, which is localized in the nucleus (Fig. 2), in COS-7 cells and evaluated β-catenin levels and its phosphorylation status in the nucleus. Expression of ΔN-GSK-3α-GFP significantly decreased nuclear β-catenin levels (Fig.

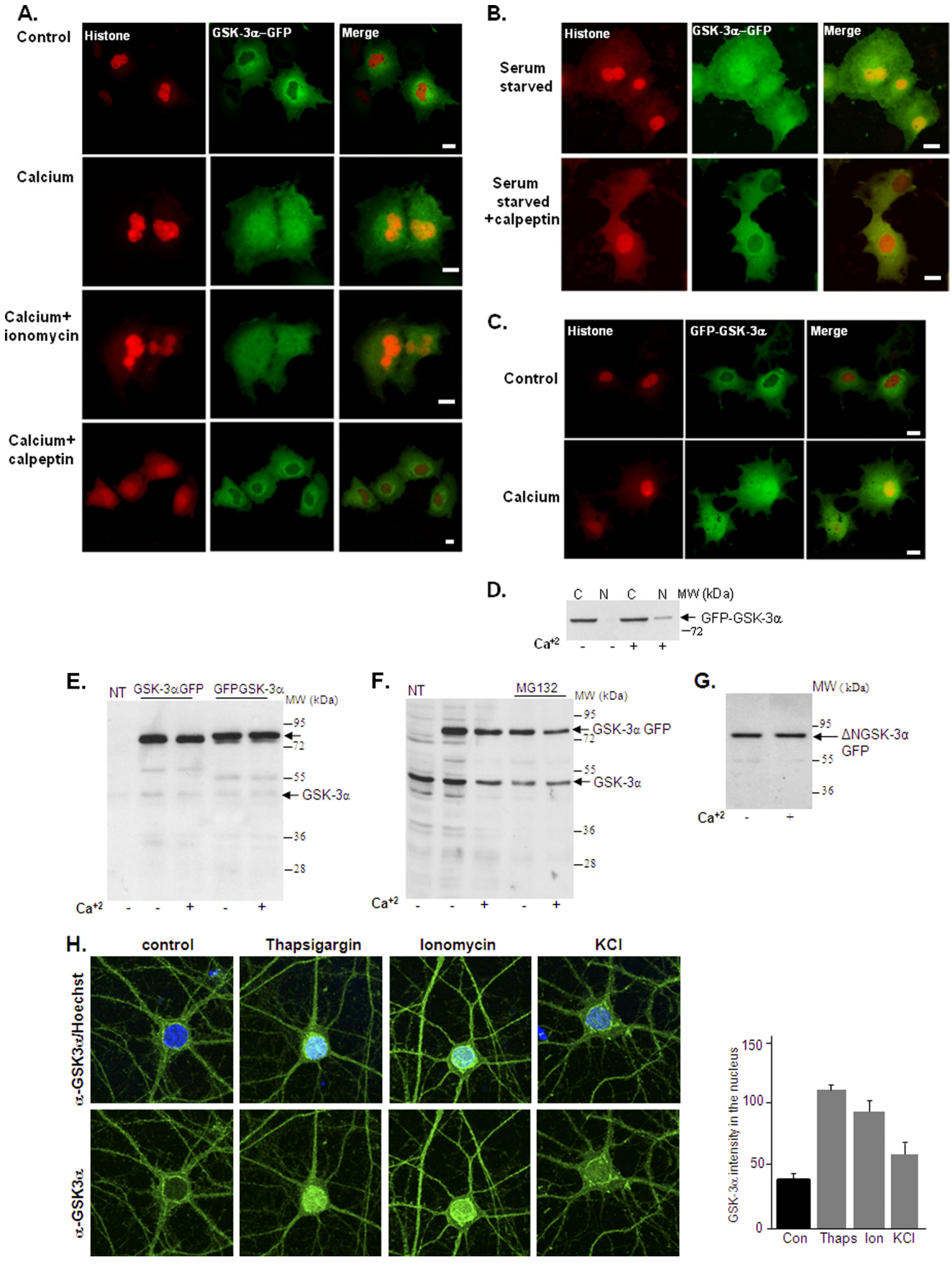
A.
Control
Histone
GSK-3α–GFP
Merge
Calcium
Calcium+ ionomycin
Calcium+ calpeptin
B.
Serum starved
Serum starved +calpeptin
C.
GFP-GSK-3α
Control
Calcium
D.
C N C N MW (kDa)
GFP-GSK-3α
72
Ca+2 - - + +
E.
NT GSK-3αGFP GFPGSK-3α
MW (kDa)
95
72
55
GSK-3α
36
28
Ca+2 - - + - +
F.
NT MG132
MW (kDa)
95
GSK-3α GFP
72
55
GSK-3α
36
28
Ca+2 - - + - +
G.
MW (kDa)
95
ΔNGSK-3α GFP
55
36
Ca+2 - +
H.
control
Thapsigargin
Ionomycin
KCl
α-GSK3α/Hoechst
α-GSK3α
GSK-3α intensity in the nucleus
150
100
50
0
Con
Thaps
Ion
KCl

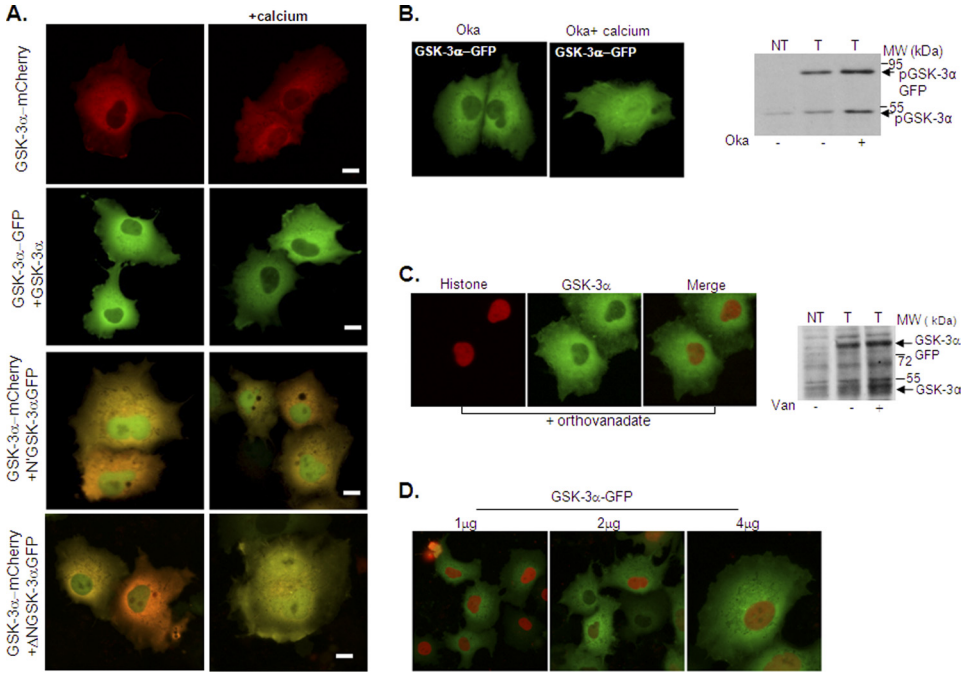

FIGURE 5. **The N-terminal region is required for calcium-induced GSK-3α nuclear accumulation.** *A*, overexpression with GSK-3α or N′-GSK-3α-GFP abolishes calcium-induced GSK-3α nuclear accumulation. COS-7 cells were co-transfected with GSK-3α-GFP and pMT2-GSK-3α constructs in a 1:2 DNA ratio, respectively. Cells were treated with 2 mM calcium, and live cells were imaged by confocal microscopy 30 min after treatment. Fluorescence of GSK-3α-GFP is shown (second panel from top). A control showing nuclear accumulation of GSK-3α-mCherry induced by calcium treatment is shown in the *top panel*. Similar experiments were performed in COS-7 cells that were co-transfected with a combination of GSK-3α-mCherry with N′-GSK-3α-GFP or with ΔN-GSK-3α-GFP (*third* and *fourth panels* from *top*, respectively). Merged GFP and mCherry fluorescence is shown. *Scale bars*, 10 μm. *B*, COS-7 cells expressing GSK-3α-GFP were treated with 100 nM okadaic acid (*Oka*) for 1 h or with 2 mM calcium added following okadaic acid treatment. Live cells were imaged by confocal microscopy (*right panel*, *upper row*). Western blot analysis using anti-phosphoserine 21 GSK-3α antibody verified increased serine phosphorylation of GSK-3α-GFP in the okadaic acid-treated cells (*right panel*, *lower row*). *NT*, nontransfected; *T*, transfected. GSK-3α-GFP and endogenous GSK-3α are indicated. *C*, images are similar to *B* except that cells were treated with sodium orthovanadate (100 nM) for 1 h, and Western blot analysis used anti-phosphotyrosine 279 GSK-3 antibody to verify the increase in tyrosine phosphorylation (*bottom row*). *Van*, orthovanadate. *D*, COS-7 cells were transfected with increasing doses of GSK-3α-GFP plasmids together with DiHcRED. Live cells were imaged by confocal microscopy as described. Fluorescence of DiHcRED and GFP and merged images are shown. Overexpressed GSK-3α resided in the cytoplasm.

6*A*). We showed that this reduction was in the "active " nonphosphorylated form of β-catenin using the ABC antibody (29) (Fig. 6*A*). Reduction in β-catenin was accompanied by a significant reduction in the expression levels if target cyclin D1 (53, 54) (Fig. 6*A*), indicating inhibition in β-catenin transcriptional activity.

We then evaluated the effect of calcium and GSK-3α on nuclear β-catenin. COS-7 cells were transfected with GSK-3α-GFP and then treated with calcium for 1 h to allow nuclear localization of GSK-3α-GFP. Reduction in nuclear β-catenin levels and its nonphosphorylated form was observed in the GSK-3α-GFP-expressing cells that were treated with calcium (Fig. 6*B*). In addition, overexpression of GSK-3α-GFP reduced cyclin D1 levels in calcium-treated cells (Fig. 6*B*). Notably, there was a small but a significant elevation in cyclin D1 levels after calcium treatment (Fig. 6*B*). It is possible that elevation in cyclin D1 resulted from calpain-mediated generation of N-terminal-truncated active forms of β-catenin with potent transcriptional activity (55). In the cytoplasm, overexpression of GSK-3α-GFP did not reduce β-catenin levels in response to calcium, indicating that phosphorylation of β-catenin is likely initiated in the nucleus (Fig. 6*C*). Similar results were obtained with nontagged GSK-3α (data not shown). Finally, we showed that although overexpression of GSK-3β-GFP reduced nuclear levels of

FIGURE 4. **Calpain mediates GSK-3α nuclear accumulation.** *A*, COS-7 cells co-transfected with GSK-3α-GFP and DiHcRED-histone plasmids were treated with 2 mM calcium or a combination of 2 mM calcium and 2 μM ionomycin. Alternatively, cells were pretreated with 50 μM calpeptin prior to calcium addition. Live cells were imaged by confocal microscopy 30 min after treatment. Fluorescence of DiHcRED and GFP and merged images are shown. *Scale bars*, 10 μm. *B*, COS-7 cells co-transfected with GSK-3α-GFP and DiHcRED-histone plasmids were serum-deprived (0.1% FCS) for 30 min. Live cells were imaged by confocal microscopy. Fluorescence of DiHcRED and GFP and merged images are shown. *C*, images are as in *A* except that GFP-GSK-3α construct was used and cells were treated with 2 mM calcium. *D*, COS-7 cells transfected with GFP-GSK-3α were treated with 2 mM calcium for 30 min. Cells were separated into nuclear (*N*) and cytosolic (*C*) fractions as described under "Experimental Procedures," and proteins were separated by gel electrophoresis followed by immunoblot analysis using anti-GFP antibody. The presence of GFP-GSK-3α protein in the nucleus indicates that full-length GSK-3α was translocated into the nucleus. No fragmentation of GFP-GSK-α was detected. *E*, COS-7 cells transfected with GSK-3α-GFP or GFP-GSK-3α constructs were treated with 2 mM calcium for 1 h. Proteins were subjected to gel electrophoresis followed by immunoblot analysis using anti-GSK-3α antibody as indicated. No GSK-3α fragmentation was detected. Endogenous GSK-3α is indicated. *NT*, nontransfected. *F*, COS-7 cells transfected with GSK-3α-GFP were pretreated with 30 μM MG132 5 h prior to the addition of 2 mM calcium. After 30 min, cells were lysed, and proteins were subjected to gel electrophoresis followed by immunoblot analysis using anti-GSK-3α antibody. No accumulation of GSK-3α fragments was detected. Endogenous GSK-3α is indicated. *G*, image is the same as in *E* except that cells were transfected with ΔN-GSK-3α-GFP. *H*, DIV21 hippocampal neurons were treated with 5 μM ionomycin for 30 min, with 2 μM thapsigargin for 45 min, or with 90 mM KCl (3 min plus 30 min in conditioned medium) to induce an increase in intracellular Ca^{2+} levels. Cells were fixed and immunostained for GSK-3α as described under "Experimental Procedures." Maximum projections of confocal *z*-stacks are presented. Quantitation of GSK-3α fluorescence in the nucleus is shown in the *right panel* and presents mean of three independent experiments ±S.E. (*error bars*).

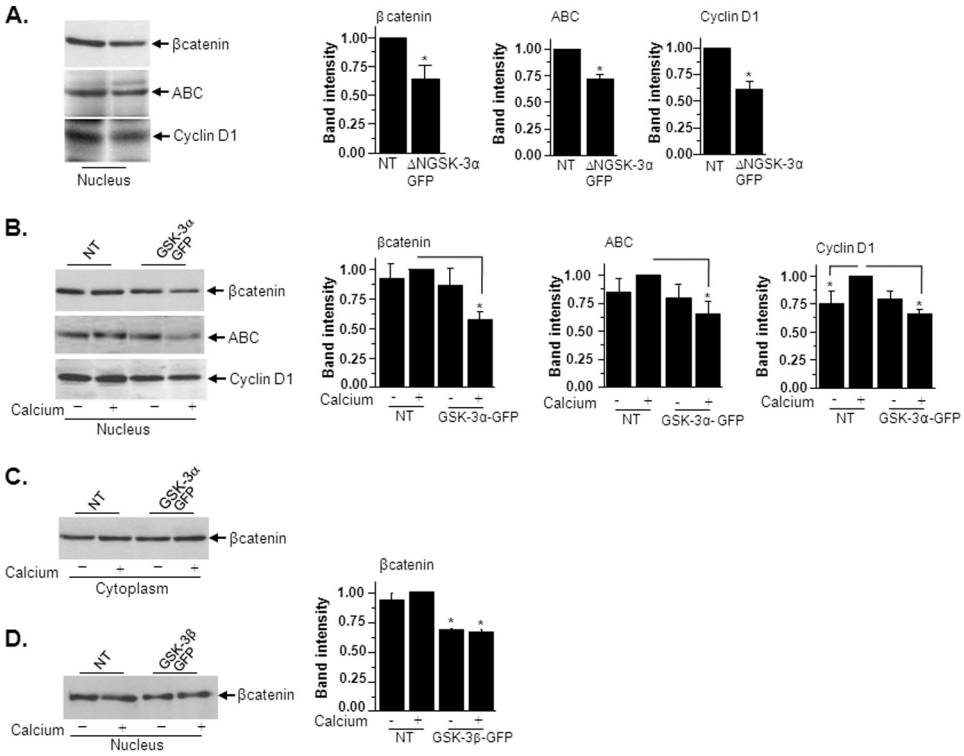

FIGURE 6. **Nuclear localization of GSK-3α destabilizes nuclear β-catenin.** *A*, COS-7 cells were transfected with ΔN-GSK-3α-GFP plasmid. Cells were fractionated into nuclear and cytosolic fractions, and nuclear proteins were separated by gel electrophoresis and immunoblotted with anti-β-catenin, ABC, and anti-cyclin D1 antibodies. Densitometry analysis of respected bands is presented as -fold of calcium treated that was designated as 1. Shown is the mean of three independent experiments ±S.E. (*error bars*). *, $p < 0.01$. *B*, COS-7 cells were transfected with GSK-3α-GFP plasmid. Cells were treated with calcium (2 mM, 1 h). β-Catenin and cyclin D1 were analyzed as described in *A*. Densitometry analysis of respected bands is shown in the *right panel* and as described in *A*. *, $p < 0.01$. *C*, shown are cytoplasmic levels of β-catenin from experiments described in *B*. *D*, COS-7 cells were transfected with GSK-3β-GFP plasmid. Cells were fractionated into nuclear and cytosolic fractions, and nuclear proteins were separated by gel electrophoresis and immunoblotted with anti-β-catenin antibody as described. Densitometry analysis of respected bands is shown in the *right panel* and as described. *NT*, nontransfected; *ABC*, anti-dephospho-βcatenin.

β-catenin (as expected), treatment with calcium did not augment this effect (Fig. 6*D*). Taken together, our data showed that GSK-3α has a specific role in regulating nuclear β-catenin in response to calcium.

DISCUSSION

In this work, we identified distinct molecular and cellular characteristics of GSK-3 isozymes. We showed that, in contrast to GSK-3β, which partitions between the cytoplasm and nucleus in a steady state, GSK-3α is apparently excluded from the nucleus. Yet, GSK-3α accumulated in the nucleus via activation of the calcium/calpain pathway or upon serum starvation. We showed that the N-terminal domain of GSK-3α, which differs substantially from that of GSK-3β, is responsible for GSK-3α nuclear exclusion. Accumulation of GSK-3α in the nucleus is mediated via GSK-3α binding with a calpain-sensitive product via its N-terminal region. Finally, we showed that nuclear localization of GSK-3α results in destabilization of nuclear β-catenin.

Analysis of the amino acid sequence of GSK-3α did not reveal any known nuclear import or export sequences. Moreover, expression of the N-terminal region (1–63 amino acids) alone did not result in any specific localization, suggesting that this domain does not contain cellular targeting sequences. GSK-3α-GFP did accumulate in the nucleus when cells were treated with leptomycin B (Fig. 2), and competition with overexpressed GSK-3α indicated that the protein is not anchored in the cytoplasm (Fig. 1 and Fig. 5, *A* and *D*). Our results favored the interpretation that the N-terminal region is responsible for the nuclear exclusion of GSK-3α.

How precisely GSK-3α accumulates in the nucleus in response to calcium is not fully known at this point. The simplest explanation is a direct calpain-mediated N-terminal truncation of GSK-3α resulting in nuclear accumulation of GSK-3α; this is supported by our result that tagged and nontagged ΔN-GSK-3α was nuclear (Fig. 2). However, further experiments showed that this mechanism is unlikely. We did not detect GSK-3α fragmentation after calcium treatment using different GFP-tagged GSK-3α constructs or after treatment with the proteasome inhibitor MG132 (Fig. 4*F*). The fact that intact GFP-GSK-3α was found in the nucleus after calcium treatment provided strong evidence that N-terminal truncation is not involved (Fig. 4*C*, Fig. 4*E*). Our observation that calpain does not induce cleavage of GSK-3α is consistent with previous reports showing that GSK-3α (compared with GSK-3β) is a poor calpain substrate (23) and that GSK-3α truncation is not detected in NMDA-treated neurons (56). We propose an alternative mechanism in which GSK-3α nuclear exclusion mediated by its N-terminal is disturbed by calpain action. Following calpain activation, GSK-3α binds with a calpain-sensitive protein or proteins enabling GSK-3α nuclear accumulation (Fig. 5*A*). This binding is mediated through the N-terminal region (Fig. 5*A*) and presumably masks the nuclear exclusion influence

of the N-terminal domain. Future studies will uncover the identity of the protein partner(s) that interact with GSK-3α following calcium/calpain activation and whether complex formation occurs in the cytoplasm or nucleus.

Previous work showed that nuclear localization of GSK-3β could be manipulated by alterations in cell cycle progression, apoptosis, Wnt signaling, and nuclear export by FRAT (57–61). One study identified an arginine motif within the catalytic domain of GSK-3β that functioned as a nuclear localization signal (62). Interestingly, deletion of the N-terminal region of GSK-3β reduced its accumulation in the nucleus (62). Hence, it is most likely that the mechanisms regulating GSK-3α nuclear accumulation differ from those that govern the nuclear localization of GSK-3β reported in the previous study.

Our bioinformatics analyses indicated that the role of the N-terminal region of GSK-3α has emerged in the course of evolution and that the isoform has acquired specific functions in mammals. We showed that features that specify cytoplasmic retention of the protein are not present in zebrafish GSK-3α, a protein that differs in its N-terminal amino acid composition from mammalian GSK-3α proteins (43) (Fig. 3). Hence, a major difference between GSK-3α and GSK-3β is the signaling-dependent localization of GSK-3α in the nucleus. The role played by the two isoforms once in the nucleus may be similar or distinct. In this work we show that GSK-3α regulates β-catenin expression in the nucleus after calcium treatment of cells. Thus, although GSK-3α and GSK-3β are functionally redundant in regulating cytoplasmic β-catenin (20), their abilities to affect β-catenin levels in the nucleus are significantly different.

The tightly regulated cellular distribution of GSK-3α may provide a unique means of controlling the specificity, timing, and strength of the calcium signal. In this respect, it is interesting to note that a rise in calcium influx has been implicated in synapse-to-nucleus communication regulating neuronal development, plasticity, and survival (63, 64). This communication has been shown to be mediated by nuclear import of cytosolic proteins such as CREB, Jacob neuroprotein, NF-ATc, NFκB, and Abelson interacting protein-1 (abi-1), which activate certain gene expression programs (65–70). Proteases, in particular calpain, play important roles in these cellular activities (66, 71). GSK-3α may thus link cytoplasmic calcium/calpain signaling with nuclear events. The example demonstrated here linked calcium signal with GSK-3α-mediated destabilization of the nuclear pool of β-catenin, thus evoking inhibition of the Wnt signaling pathway (Fig. 6). This suggested a new paradigm in which calcium signaling is linked with the canonical Wnt/β-catenin via GSK-3α. This hypothesis is further supported by recent work that has revealed network connections in Wnt signaling pathways (72). It is interesting to note that malactivation of the calcium/calpain signal has been implicated in pathological conditions associated with cell damage, cell death, and neurological disorders, including Alzheimer disease (25–27, 73). It is tempting to speculate that abnormal accumulation of GSK-3α in the nucleus mediates, at least in part, these pathological disorders through inhibition of expression of nuclear β-catenin, as demonstrate with our nuclear-localized construct ΔN-GSK-3α (Fig. 6*A*). In summary, we provide novel insights into the role of the N-terminal region of GSK-3. We further uncovered a novel link between calcium/calpain signaling and GSK-3α-mediated inhibition of the canonical Wnt/β-catenin pathway.

REFERENCES

1. Grimes, C. A., and Jope, R. S. (2001) *Prog. Neurobiol.* **65,** 391–426
2. Doble, B. W., and Woodgett, J. R. (2003) *J. Cell Sci.* **116,** 1175–1186
3. Frame, S., and Cohen, P. (2001) *Biochem. J.* **359,** 1–16
4. Eldar-Finkelman, H. (2002) *Trends Mol. Med.* **8,** 126–132
5. Gould, T. D., Zarate, C. A., and Manji, H. K. (2004) *J. Clin. Psychiatry* **65,** 10–21
6. Muntané, G., Dalfó, E., Martinez, A., and Ferrer, I. (2008) *Neuroscience* **152,** 913–923
7. Jope, R. S., Yuskaitis, C. J., and Beurel, E. (2007) *Neurochem. Res.* **32,** 577–595
8. Schloesser, R. J., Huang, J., Klein, P. S., and Manji, H. K. (2008) *Neuropsychopharmacology* **33,** 110–133
9. Huang, H. C., and Klein, P. S. (2006) *Curr. Drug Targets* **7,** 1389–1397
10. Rowe, M. K., Wiest, C., and Chuang, D. M. (2007) *Neurosci. Biobehav. Rev.* **31,** 920–931
11. Woodgett, J. R. (1990) *EMBO J.* **9,** 2431–2438
12. Wang, Q. M., Park, I. K., Fiol, C. J., Roach, P. J., and DePaoli-Roach, A. A. (1994) *Biochemistry* **33,** 143–147
13. Hoeflich, K. P., Luo, J., Rubie, E. A., Tsao, M. S., Jin, O., and Woodgett, J. R. (2000) *Nature* **406,** 86–90
14. MacAulay, K., Doble, B. W., Patel, S., Hansotia, T., Sinclair, E. M., Drucker, D. J., Nagy, A., and Woodgett, J. R. (2007) *Cell Metab.* **6,** 329–337
15. Patel, S., Doble, B. W., MacAulay, K., Sinclair, E. M., Drucker, D. J., and Woodgett, J. R. (2008) *Mol. Cell. Biol.* **28,** 6314–6328
16. Phiel, C. J., Wilson, C. A., Lee, V. M., and Klein, P. S. (2003) *Nature* **423,** 435–439
17. Kerkela, R., Kockeritz, L., Macaulay, K., Zhou, J., Doble, B. W., Beahm, C., Greytak, S., Woulfe, K., Trivedi, C. M., Woodgett, J. R., Epstein, J. A., Force, T., and Huggins, G. S. (2008) *J. Clin. Invest.* **118,** 3609–3618
18. Force, T., and Woodgett, J. R. (2009) *J. Biol. Chem.* **284,** 9643–9647
19. Liang, M. H., and Chuang, D. M. (2006) *J. Biol. Chem.* **281,** 30479–30484
20. Doble, B. W., Patel, S., Wood, G. A., Kockeritz, L. K., and Woodgett, J. R. (2007) *Dev. Cell* **12,** 957–971
21. Zhou, F. Q., Zhou, J., Dedhar, S., Wu, Y. H., and Snider, W. D. (2004) *Neuron* **42,** 897–912
22. Kim, W. Y., Zhou, F. Q., Zhou, J., Yokota, Y., Wang, Y. M., Yoshimura, T., Kaibuchi, K., Woodgett, J. R., Anton, E. S., and Snider, W. D. (2006) *Neuron* **52,** 981–996
23. Goñi-Oliver, P., Lucas, J. J., Avila, J., and Hernández, F. (2007) *J. Biol. Chem.* **282,** 22406–22413
24. Goll, D. E., Thompson, V. F., Li, H., Wei, W., and Cong, J. (2003) *Physiol. Rev.* **83,** 731–801
25. Chong, Z. Z., Li, F., and Maiese, K. (2005) *Prog. Neurobiol.* **75,** 207–246
26. Johnson, G. V. (2006) *J. Alzheimers Dis.* **9,** 243–250
27. Bertipaglia, I., and Carafoli, E. (2007) *Subcell. Biochem.* **45,** 29–53
28. Benetti, R., Copetti, T., Dell'Orso, S., Melloni, E., Brancolini, C., Monte, M., and Schneider, C. (2005) *J. Biol. Chem.* **280,** 22070–22080
29. Staal, F. J., Noort Mv, M., Strous, G. J., and Clevers, H. C. (2002) *EMBO Rep.* **3,** 63–68
30. Li, G., and Iyengar, R. (2002) *Proc. Natl. Acad. Sci. U.S.A.* **99,** 13254–13259
31. Peifer, M., and Polakis, P. (2000) *Science* **287,** 1606–1609
32. Bienz, M. (2005) *Curr. Biol.* **15,** R64–67
33. Yost, C., Torres, M., Miller, J. R., Huang, E., Kimelman, D., and Moon, R. T. (1996) *Genes Dev.* **10,** 1443–1454
34. Liu, C., Li, Y., Semenov, M., Han, C., Baeg, G. H., Tan, Y., Zhang, Z., Lin, X., and He, X. (2002) *Cell* **108,** 837–847
35. Peifer, M., Pai, L. M., and Casey, M. (1994) *Dev. Biol.* **166,** 543–556
36. Dajani, R., Fraser, E., Roe, S. M., Young, N., Good, V., Dale, T. C., and Pearl, L. H. (2001) *Cell* **105,** 721–732
37. Dukhovny, A., Papadopulos, A., and Hirschberg, K. (2008) *J. Cell Sci.* **121,** 865–876
38. Altschul, S. F., Madden, T. L., Schäffer, A. A., Zhang, J., Zhang, Z., Miller,

W., and Lipman, D. J. (1997) *Nucleic Acids Res.* **25,** 3389–3402
39. Bailey, T. L., and Elkan, C. (1994) *Proc. Int. Conf. Intell. Syst. Mol. Biol.* **2,** 28–36
40. Frith, M. C., Saunders, N. F., Kobe, B., and Bailey, T. L. (2008) *PLoS Comput. Biol.* **4,** e1000071
41. Henikoff, S., Henikoff, J. G., Alford, W. J., and Pietrokovski, S. (1995) *Gene* **163,** GC17–26
42. Banker, G., and Goslin, K. (1991) pp. xiii, 453, MIT Press, Cambridge, MA
43. Goslin, K., and Banker, G. (1991) in *Culturing Nerve Cells* (Banker, G., and Goslin, K., eds) pp. 251–281, MIT Press, Cambridge, MA
44. Cho, J., Rameshwar, P., and Sadoshima, J. (2009) *J. Biol. Chem.* **284,** 36647–36658
45. Adachi, M., Fukuda, M., and Nishida, E. (1999) *EMBO J.* **18,** 5347–5358
46. Khokhlatchev, A. V., Canagarajah, B., Wilsbacher, J., Robinson, M., Atkinson, M., Goldsmith, E., and Cobb, M. H. (1998) *Cell* **93,** 605–615
47. Raman, M., and Cobb, M. H. (2003) *Curr. Biol.* **13,** R886–888
48. Bendetz-Nezer, S., and Seger, R. (2007) *J. Biol. Chem.* **282,** 25114–25122
49. Sutherland, C., and Cohen, P. (1994) *FEBS Lett.* **338,** 37–42
50. Frame, S., Cohen, P., and Biondi, R. M. (2001) *Mol. Cell* **7,** 1321–1327
51. Hughes, K., Nikolakaki, E., Plyte, S. E., Totty, N. F., and Woodgett, J. R. (1993) *EMBO J.* **12,** 803–808
52. Aberle, H., Bauer, A., Stappert, J., Kispert, A., and Kemler, R. (1997) *EMBO J.* **16,** 3797–3804
53. Tetsu, O., and McCormick, F. (1999) *Nature* **398,** 422–426
54. Shtutman, M., Zhurinsky, J., Simcha, I., Albanese, C., D'Amico, M., Pestell, R., and Ben-Ze'ev, A. (1999) *Proc. Natl. Acad. Sci. U.S.A.* **96,** 5522–5527
55. Abe, K., and Takeichi, M. (2007) *Neuron* **53,** 387–397
56. Goñi-Oliver, P., Avila, J., and Hernández, F. (2009) *J. Alzheimers Dis.* **18,** 843–848
57. Diehl, J. A., Cheng, M., Roussel, M. F., and Sherr, C. J. (1998) *Genes Dev.* **12,** 3499–3511
58. Bijur, G. N., De Sarno, P., and Jope, R. S. (2000) *J. Biol. Chem.* **275,** 7583–7590
59. Bijur, G. N., and Jope, R. S. (2003) *Neuroreport* **14,** 2415–2419
60. Caspi, M., Zilberberg, A., Eldar-Finkelman, H., and Rosin-Arbesfeld, R. (2008) *Oncogene* **27,** 3546–3555
61. Franca-Koh, J., Yeo, M., Fraser, E., Young, N., and Dale, T. C. (2002) *J. Biol. Chem.* **277,** 43844–43848
62. Meares, G. P., and Jope, R. S. (2007) *J. Biol. Chem.* **282,** 16989–17001
63. Greer, P. L., and Greenberg, M. E. (2008) *Neuron* **59,** 846–860
64. Jordan, B. A., and Kreutz, M. R. (2009) *Trends Neurosci.* **32,** 392–401
65. Dash, P. K., Karl, K. A., Colicos, M. A., Prywes, R., and Kandel, E. R. (1991) *Proc. Natl. Acad. Sci. U.S.A.* **88,** 5061–5065
66. Lai, K. O., Zhao, Y., Ch'ng, T. H., and Martin, K. C. (2008) *Proc. Natl. Acad. Sci. U.S.A.* **105,** 17175–17180
67. Dieterich, D. C., Karpova, A., Mikhaylova, M., Zdobnova, I., König, I., Landwehr, M., Kreutz, M., Smalla, K. H., Richter, K., Landgraf, P., Reissner, C., Boeckers, T. M., Zuschratter, W., Spilker, C., Seidenbecher, C. I., Garner, C. C., Gundelfinger, E. D., and Kreutz, M. R. (2008) *PLoS Biol.* **6,** e34
68. Graef, I. A., Mermelstein, P. G., Stankunas, K., Neilson, J. R., Deisseroth, K., Tsien, R. W., and Crabtree, G. R. (1999) *Nature* **401,** 703–708
69. Meffert, M. K., Chang, J. M., Wiltgen, B. J., Fanselow, M. S., and Baltimore, D. (2003) *Nat. Neurosci.* **6,** 1072–1078
70. Proepper, C., Johannsen, S., Liebau, S., Dahl, J., Vaida, B., Bockmann, J., Kreutz, M. R., Gundelfinger, E. D., and Boeckers, T. M. (2007) *EMBO J.* **26,** 1397–1409
71. Kindler, S., Dieterich, D. C., Schütt, J., Sahin, J., Karpova, A., Mikhaylova, M., Schob, C., Gundelfinger, E. D., Kreienkamp, H. J., and Kreutz, M. R. (2009) *J. Biol. Chem.* **284,** 25431–25440
72. Kestler, H. A., and Kühl, M. (2008) *Philos. Trans. R Soc. Lond. B Biol. Sci.* **363,** 1333–1347
73. Lee, M. S., Kwon, Y. T., Li, M., Peng, J., Friedlander, R. M., and Tsai, L. H. (2000) *Nature* **405,** 360–364